Input-output curves of low and high spontaneous rate auditory nerve fibers are exponential near threshold

Horst, J. Wiebe; McGee, JoAnn; Walsh, Edward J.

Published in:
Hearing Research

DOI:
10.1016/j.heares.2018.06.007

Hearing Research 367 (2018) 195–206

Contents lists available at ScienceDirect

Hearing Research

journal homepage: www.elsevier.com/locate/heares

Research Paper

Input-output curves of low and high spontaneous rate auditory nerve fibers are exponential near threshold☆

J. Wiebe Horst [a, *], JoAnn McGee [b, 1], Edward J. Walsh [b, 1]

[a] University of Groningen, University Medical Center Groningen, Department of Otorhinolaryngology/Head and Neck Surgery, P.O. Box 30.001, 9700 RB Groningen, the Netherlands
[b] Boys Town National Research Hospital, 555 North 30th Street, Omaha, NE 68131, USA

ARTICLE INFO

Article history:
Received 30 September 2017
Received in revised form
12 June 2018
Accepted 12 June 2018
Available online 4 July 2018

Keywords:
Cochlea
Auditory nerve fibers
Spontaneous discharge rate
Instantaneous discharge rate
Period histograms
Input-output relation

ABSTRACT

Input-output (IO) properties of cochlear transduction are frequently determined by analyzing the average discharge rates of auditory nerve fibers (ANFs) in response to relatively long tonal stimulation. The ANFs in cats have spontaneous discharge rates (SRs) that are bimodally distributed, peaking at low (<0.5 spikes/s) and high (~60 spikes/s) rates, and rate-level characteristics differ depending upon SR. In an effort to assess the instantaneous IO properties of ANFs having different SRs, static IO-curves were constructed from period histograms based on phase-locking of spikes to the stimulus waveform. These curves provide information unavailable in conventional average rate-level curves. We find that all IO curves follow an exponential trajectory. It is argued that the exponential behavior represents the transduction in the IHC and that the difference among ANFs having different SRs is predominantly a difference in gain attributed most likely to synaptic drive.

1. Introduction

Trains of spikes of primary afferent auditory nerve fibers (ANFs) encode sensory information transduced within the inner ear, and information about the acoustic stimulus is relayed with high fidelity to the central nervous system. Morphologically, ANFs can be classified into large and myelinated type I ANFs that contact the pillar side of inner hair cells (IHCs), smaller myelinated type I ANFs that contact the modiolar side of IHCs and small, unmyelinated type II ANFs that innervate the outer hair cells (OHCs) (Spoendlin, 1973; Liberman, 1980). The majority of ANFs (90–95%) are type I ANFs and each type I ANF contacts a single IHC in the domestic cat. The number of ANFs contacting each IHC peaks at approximately 30 in the vicinity of the 10 kHz region and decreases progressively to about 10 for apical hair cells (Spoendlin, 1973; Liberman et al., 1990). On physiological grounds, ANFs can be classified according to a variety of criteria, including spontaneous discharge rate (SR). SRs of ANFs in deeply anesthetized cats vary from near zero to about 100 spikes/s, with approximately 60% exhibiting high SRs (SR > 17.5 spikes/s), 25–30% exhibiting medium SRs (0.5 spikes/s ≤ SR ≤ 17.5 spikes/s) and 10–15% exhibiting low SRs (SR < 0.5 spikes/s). Each IHC is contacted by low, medium and high SR ANFs (Liberman, 1982; Wu et al., 2016).

As part of the larger effort to understand the processing of sounds by the auditory periphery, inner ear input-output (IO) relationships have been assessed traditionally by measuring average discharge rates produced by type I ANFs in response to relatively long duration periodic signals, including both tone-burst and spectrally complex acoustic stimuli (e.g. Kiang et al., 1965; Rose et al., 1967; Johnson, 1980; McGee, 1983; Horst et al., 1990). In general, average discharge rates increase sigmoidally with increasing sound stimulation level, exhibiting either a saturating or a sloping shape at high levels for ANFs with high- and low-SRs, respectively (Sachs and Abbas, 1974; Winter et al., 1990; Yates et al., 1990). Information contained in such rate-level curves is limited by the fact that response variations observed within a

☆ Parts of this paper were presented at the 17th and 30th Midwinter meetings of the Association for Research in Otolaryngology in 1994 and 2007 and the 42nd and 44th Workshop on Inner Ear Biology in 2005 and 2007.

* Corresponding author.
E-mail address: wiebe.horst@gmail.com (J.W. Horst).
[1] Current address: University of Minnesota Twin Cities, CLA-Speech-Language-Hearing Sciences and Center for Applied and Translational Sensory Science, Minneapolis, MN 55455, U.S.A.

https://doi.org/10.1016/j.heares.2018.06.007
0378-5955/

stimulus period are not represented, in contrast with information contained in period histograms. A period histogram is a graph of the instantaneous discharge rate plotted on a time scale modulo the stimulus period. As a consequence, spike occurrences within a period histogram provide information on the relation between instantaneous stimulus pressure and instantaneous discharge rate.

Numerous studies have shown differences in the responses of low- and high-SR ANFs. For example, expansive nonlinear behavior has been observed at low stimulus levels in responses of ANFs with relatively low SRs (Geisler, 1990). Kiang et al. (1965) and Geisler and Silkes (1991) found that peristimulus time histograms (PST) were more deeply modulated for low-SR ANFs than for high-SR ANFs in response to the fundamental frequency of periodic complex tones. In addition, low-SR ANFs produce higher synchronization indices in response to pure tones than do high-SR ANFs (Johnson, 1980; McGee, 1983; Joris et al., 1994; Dreyer and Delgutte, 2006; Temchin and Ruggero, 2010). Similarly, Horst et al. (1986a, 1990) found a lack of response to small peaks in the temporal waveforms of complex stimuli in ANFs with relatively low SR. Geisler (1990) has suggested fundamental differences in rate-level curves between ANFs with low SR and ANFs with high SR.

On the other hand, work by Kiang et al. (1965) and Evans (1968) has suggested that the relation between instantaneous discharge rate and instantaneous stimulus pressure for ANFs of all SRs can be represented by an exponential function. This relation has been used successfully in modeling work by Siebert (1970), Colburn (1973), Johnson (1974) and Goldstein and Srulovicz (1977). Consequently, there appears to be a disagreement between this early modeling work and later experimental findings indicating that differences in the response properties of low-SR ANFs and high-SR ANFs exist.

Directly comparing average discharge rate-level curves and instantaneous discharge rate-instantaneous pressure relationships is hampered by the fact that rate-level curves are based on averages of spike numbers regardless of variations in rate across the stimulus period. That is, they cannot reveal information, such as the exponential input-output curve, on a time scale shorter than the stimulus period. To overcome this, here we show input-output relations based on the variation in instantaneous rate measured within a stimulus period.

Average discharge rate and instantaneous discharge rate are both determined by measuring the number of spikes in certain intervals and determining the number of spikes per unit of time. The important difference lies in the choice of the sampling intervals. In the case of average rate, the relevant interval is the time during which the stimulus was present and the computation of average discharge rate involves averaging across repetitions of the tone burst, periods of the stimulus, and all phases within each period. In the case of instantaneous discharge rate, the computation of rate involves averaging across repetitions of the tone burst and cycles of the stimulus, but not across all phases within each cycle, just some range of phases depending on the bin width chosen. In this way, the variation of discharge rate can be measured within the stimulus period (instantaneous discharge rate) and examined as a function of the instantaneous stimulus pressure.

In this study, in an effort to investigate these different types of input-output relations, we compared the IO properties of ANFs in deeply anesthetized cats based on traditional average discharge rate-stimulus level curves with IO curves based on instantaneous discharge rate vs. instantaneous pressure derived from period histograms at near threshold stimulus conditions.

By using tone-burst stimuli, the effect of filtering (response attenuation) that occurs when there is a mismatch between the characteristic frequency (CF) of the auditory filter and stimulus frequency can be dismissed; the filter effect will not affect the shape of the waveform. This is in contrast to a complex stimulus whose components can be differentially attenuated depending on their frequency relative to the characteristic frequency of the filter.

2. Materials and methods

2.1. Surgical preparation

Data were acquired from four adult, healthy domestic cats and experiments were performed in an electrically shielded, double-walled sound attenuating chamber specially designed for acoustic isolation (Industrial Acoustics Corp.). Animals were anesthetized with sodium pentobarbital (40 mg/kg) administered intraperitoneally and supplemental doses were administered as needed throughout the experiment; i.e., when a pedal reflex was observed. Body temperature was thermostatically regulated and maintained at approximately 38 °C. The pinna of the right ear was resected to the level of the tympanic annulus, and the skin and musculature overlying the posterior aspect of the skull were reflected and the skull overlying the cerebellum was trephined, the dura mater was opened, and the cerebellum overlying the cochlear nucleus complex was aspirated. The auditory nerve was exposed by wedging small pieces of cotton between the brainstem and the internal auditory canal. A plastic Davies-type chamber was placed over the nerve, cemented into place and filled with warm mineral oil to minimize brain pulsations and prevent tissue desiccation.

The experiments were approved by the Institutional Animal Care and Use Committee at the Boys Town National Research Hospital.

2.2. Sound delivery and data acquisition

Stimuli were delivered via a Beyer DT48 dynamic earphone that was connected through a short piece of plastic tubing to an ear piece that was inserted into the external auditory meatus and sealed in place, forming a closed acoustic system. Glass electrodes filled with 3M KCl and having an AC impedance of 20–30 MΩ at 1 kHz were used to isolate and record the extracellular activity of single ANFs.

The experimental paradigm started with the determination of spontaneous rate (SR) by measuring spike activity during a 10 s “quiet” data collection window. A tuning curve was then acquired using a modification of the algorithm described by Liberman (1978). This provided estimates of the ANF's characteristic frequency (CF) and threshold determined using a criterion of 20 spikes/s above baseline rates. Average discharge rate based IO curves, usually called rate-level curves, were constructed at CF from responses to tone-burst stimuli presented at levels spanning the ANF's dynamic range, i.e. the level range over which the average rate increases from the spontaneous rate to saturation, in 5 dB increments. Tone-burst duration was one second with 5 ms rise/fall times and stimuli were presented at a rate of one per 1.5 s. Stimuli were repeated until at least 500 spikes were obtained. Levels were incremented from low to high to minimize adaptation concerns.

Period histograms were generated by plotting discharge activity modulo stimulus period. The discharge activity was represented as instantaneous rate (the number of spikes collected in a bin divided by the total time spent in that bin). Spike times were recorded at levels near discharge rate thresholds based on values obtained from tuning curves, although data were collected near synchronization threshold (based on visual inspection) when possible. A minimum of 500 spikes was acquired to permit the construction of well-defined period histograms, a process that generally required a collection time of 500/(spontaneous rate) s. Consequently, no more than 28 s of data collection time were required to obtain requisite data for high-SR ANFs, while several minutes of data collection time

were required to attain requisite data for low-SR ANFs. When the spontaneous rate was below 1/s, collection times were generally too long to determine sufficiently precise period histograms at near synchronization threshold levels, and slightly higher stimulus levels were used to meet data collection requirements.

To accurately determine the shape of IO-curves, it was necessary to divide the period histogram into the number of bins (N) that provides a sufficient level of response detail to conduct robust analyses; the selection of too few bins will result in an inadequate density of data points, impoverished data, and diminished analytical power. In Fig. 1, a series of period histograms constructed from various values of N is shown. When four bins were used to construct the period histogram (data not shown), the essential shape of the period histogram was clear, but the amount of detail was inadequate to support robust analysis. When the bin number was increased to 8, as shown in Fig. 1A, the degree of detail increased, but the form of the period histogram remained relatively crude and instantaneous rates could not be assessed in detail. However, there is good agreement between the shapes of the period histograms determined for bin numbers of 16 and 32 (Fig. 1B and C, respectively). Increasing the number of bins further can produce more detailed IO curves, although the number of spikes collected in any bin would be roughly halved as a result of doubling the N, thus increasing the influence of statistical noise (e.g., Fig. 1D). The magnitude of this effect would in turn depend on the total number of spikes collected. Thus, the optimal number of period histogram bins depends on the number of spikes collected for every period histogram. In our analysis we chose an N = 32 on the basis of practicality; that degree of binning permits the construction of detailed IO curves and avoids the statistical noise problems that accompany excessive binning.

2.3. Analysis of period histograms

Input-output curves were constructed by plotting instantaneous discharge rate as a function of instantaneous sound pressure derived from period histograms. Sound pressure was calculated by translating the sound pressure level (SPL) of the stimulus to effective pressure:

$$P_{eff} = 2 \times 10^{-5+SPL/20} \quad (1)$$

Then, the instantaneous pressure as a function of time can be written as:

$$P(t) = P_{eff} \times \sqrt{2}\sin(2\pi ft + \varphi) \quad (2)$$

In equation (2) φ is a phase angle that is inserted to bring the stimulus waveform in phase with the period histogram. In the present analysis, we treated the stimulus as having the same phase as the response; i.e., phase shifts caused by runtimes or filter characteristics were also attributed to the stimulus. This was accomplished by (1) computing the FFT of the response (waveform of the period histogram), (2) determining the fundamental component of the spectrum, and (3) using the inverse FFT of the fundamental component to recover the waveform shape of that component in phase with the period histogram. After adequate multiplication according to equation (2), this waveform was taken as the input, providing one value of instantaneous pressure for each bin. The period histogram was taken as the output. Comparing input and output bin by bin gave an estimate of the IO-curve.

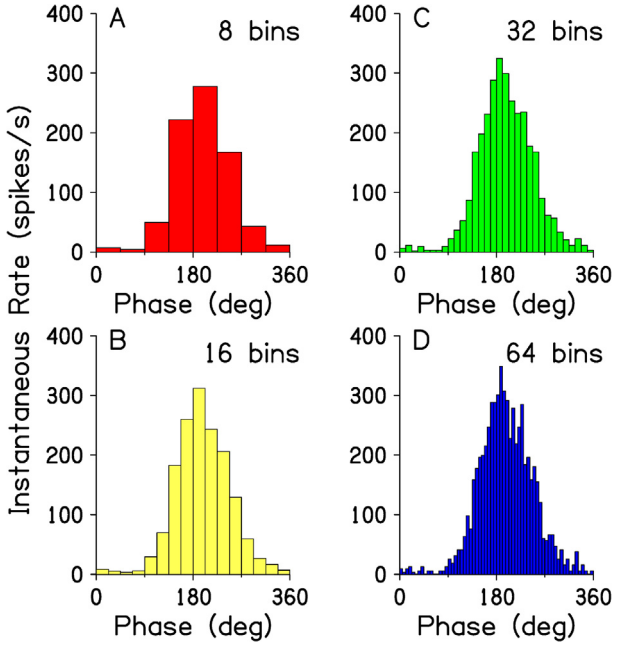

Fig. 1. Examples of period histograms and instantaneous rates using different number of histogram bins, i.e. N = 8, 16, 32, 64. The period histogram becomes more detailed for increasing values of N. For N = 64 statistical noise becomes apparent. Even for N = 8, the period histogram retains the same basic shape as period histograms with other bin numbers. The ANF had a CF of 336 Hz and spontaneous activity of 75 spikes/s. The stimulus was a tone of 336 Hz at 42 dB SPL.

3. Results

In a memoryless time-invariant system, the relation between instantaneous stimulus input and instantaneous response output can be used to characterize IO behavior by comparing the output data with the input data, as shown schematically in Fig. 2. In this investigation, the instantaneous sound pressure was the input signal and the period histogram played the role of the output signal.

Twenty-eight ANFs with CFs ranging from 0.306 to 17.3 kHz and SRs ranging from near 0.2 to 100.5 spikes/s provided the data for this study. An example of a pure-tone period histogram derived from spikes recorded from an ANF with intermediate SR (12 spk/s) at near threshold intensity is shown in Fig. 3A. The characteristic-frequency (CF) of the ANF was 700 Hz and the stimulus was

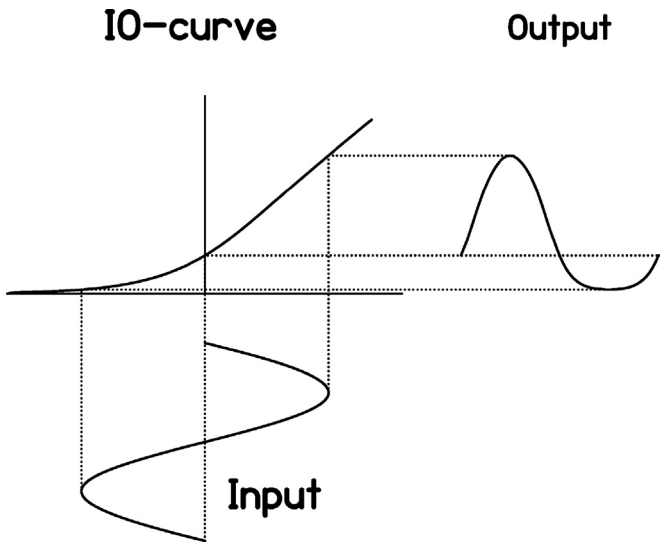

Fig. 2. Schematic diagram illustrating the relation between the input waveform and the output waveform via an input-output function. Given two of these, the third one can be constructed.

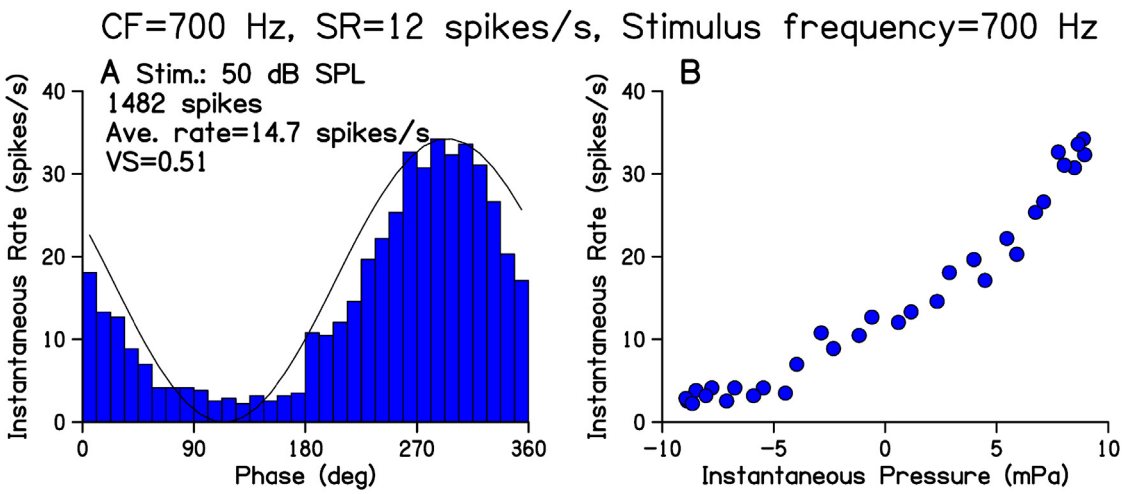

Fig. 3. A: A period histogram is shown in response to a pure tone at the CF of the ANF. On the vertical scale instantaneous rate is plotted, i.e. the number of spikes collected in each bin divided by the total time spent in that bin. A sinusoid is drawn overlying the period histogram to indicate the phase of the fundamental component of the frequency spectrum of the period histogram. B: The corresponding input-output curve for the period histogram shown in A is constructed by plotting the instantaneous discharge rate in each bin of the histogram versus the instantaneous pressure associated with the stimulus waveform. The ANF had a CF of approximately 700 Hz and spontaneous activity of 12 spikes/s. The stimulus was a pure tone of 700 Hz at 50 dB SPL, i.e. it had an amplitude of 8.944 mPa. VS represents the vector strength.

presented at 700 Hz and 50 dB SPL, i.e. 7 dB below the rate threshold.

It is clear that spike-activity was detected throughout the period (cycle) of the tone-burst and at this stimulus level the activity of the ANF can be regarded as a modulation of spontaneous activity; i.e., the average discharge rate (14.7 spikes/s) was only slightly above SR. However, it is notable that the instantaneous rate varied between 2 and 34 spikes/s depending upon stimulus phase, indicating that instantaneous discharge rate variation can be used to investigate the effect of instantaneous variation of instantaneous pressure within a stimulus period.

Based on the calculation strategy described earlier, a stimulus level of 50 dB SPL corresponds to an effective pressure of 6.325 mPa and according to equation (2) the instantaneous pressure varied between +8.944 and −8.944 mPa. In Fig. 3B, after shifting the phase to discard delays caused by consecutive transduction stages, instantaneous rate was plotted as a function of instantaneous pressure, a manipulation that collapses the relation between stimulus and response onto a single IO-curve centered on 0 mPa (the null pressure), with both positive and negative instantaneous-pressure values mapping-out the curve.

Fig. 4 shows instantaneous rates collected at three levels near threshold. These are data from an ANF with a CF of 591 Hz and a high SR (37 spikes/s). The stimulus frequency was 600 Hz. Again, firing was observed throughout the stimulus period and associated period histograms can be described as waveforms with amplitude modulation around a baseline, the SR. Increasing the stimulus level results in deeper modulation, and decreased discharge rate in one half of the period as a consequence. This is in agreement with prior work (Rose et al., 1967; Johnson, 1980).

As shown previously, plotting instantaneous rate as a function of instantaneous pressure yields an orderly series of values that vary continuously around SR (star in Fig. 4D and F). For the 35 dB SPL stimulus condition, the spread of the instantaneous rate around SR is small but consistent (Fig. 4C and F). For positive input pressures, the discharge rate is above SR, and for negative input pressures, discharge rates below SR were observed. The instantaneous discharge rate for zero input is in good agreement with SR; i.e. response for zero input in the dynamic and the static conditions agree. These observations can be made for responses to each of the stimulus levels presented here. It is noteworthy that the average rate increases marginally when the stimulus level is increased from 35 to 50 dB SPL (Fig. 4G), whereas instantaneous rates range from 7 spikes/s to over 120 spikes/s (Fig. 4H), an increase of more than a factor of 10.

In Fig. 4H, data from Fig. 4D and F are re-plotted in one frame and it is clear that static IO curves derived from different stimulus levels overlap completely, showing that data acquired from stimuli at various near threshold levels can be represented by a single IO-curve; i.e., the representation of the data by a single static nonlinearity is a robust representation in the range of stimulus levels that are presented. Restricted parts of this curve look fairly linear, but from the smallest to the largest pressures there is a definite increase in the slope of the curve, although the change in slope is not abrupt, but continuous in nature. Consequently, we do not see half-wave rectification in which there is no or hardly any response in one half of the period and a fairly linear response in the other half in this stimulation range. In all curves, the instantaneous rate at zero input pressure agrees very well with the SR, i.e. the rate when there is no stimulus at all.

Data from another ANF with a CF of 550 Hz and a low SR (0.7 spikes/s) are shown in Fig. 5. In this case, data were collected near rate threshold to limit data collection time. In the right column, IO-curves that were constructed from period histograms are shown. Again, we find smooth curves in which the instantaneous rate at zero input pressure is in excellent agreement with SR.

In the case of this low-SR ANF, data were collected at two stimulus levels and in Fig. 5D it is shown that these data are in good agreement and can be collapsed onto a single IO-curve. As in the case of the high-SR ANF considered above, the slope of the curve increases consistently and again there is no sudden change near zero input pressure.

Because the average driven rates of most ANFs saturate at higher levels (Sachs and Abbas, 1974), one goal of this investigation was to determine the effects of higher levels on the behavior of the instantaneous rates. For this reason, we considered data collected at stimulus levels well above the discharge rate threshold. Findings from an ANF with a CF of 500 Hz and with an intermediate SR (3.2 spikes/s) are shown in Fig. 6. Responses are plotted as IO-curves and, as with data presented above for the high and low-SR ANFs,

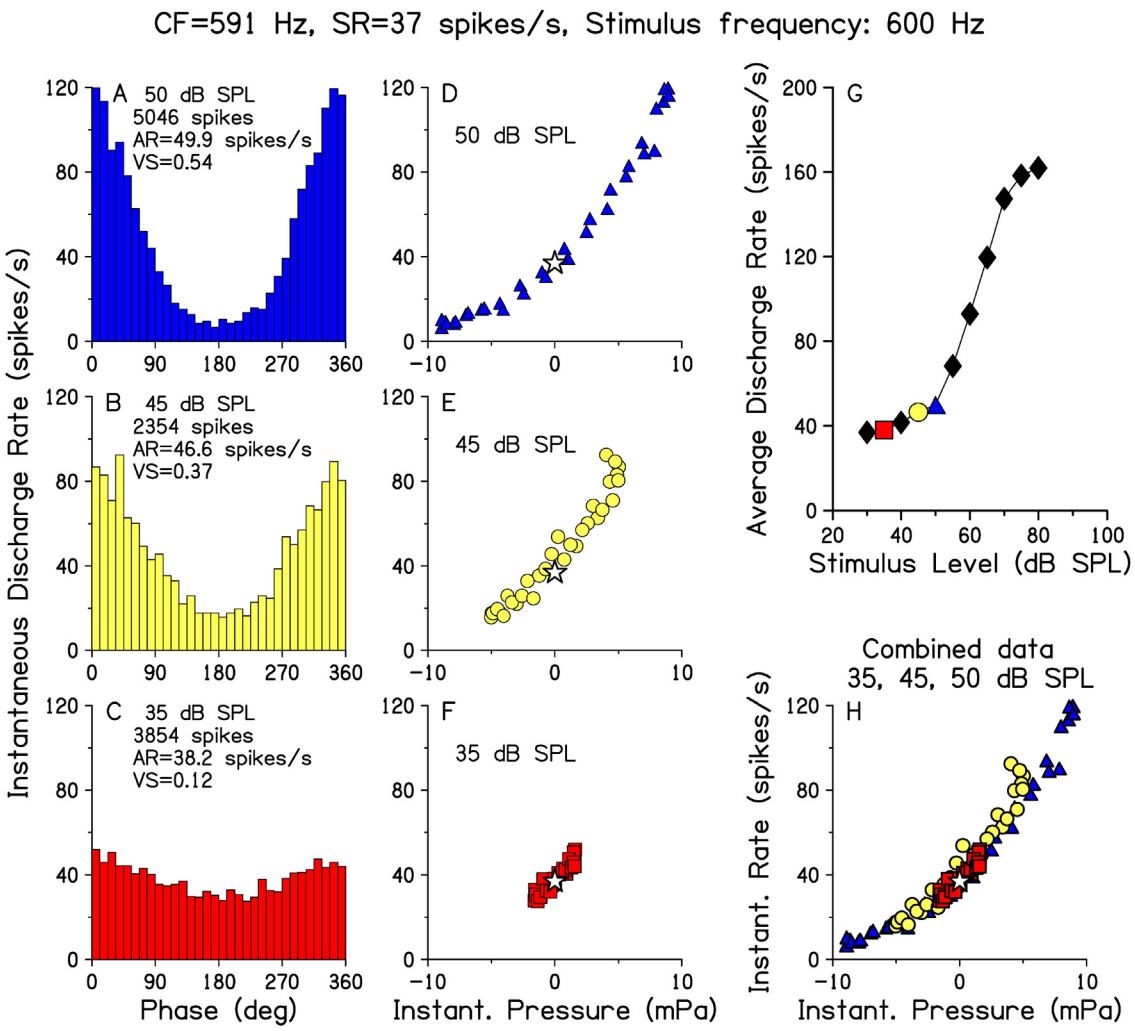

Fig. 4. Period histograms (A–C), associated IO-curves (D–F), and the average rate-level curve (G) are shown for an ANF in response to 600 Hz tone bursts. Period histograms and IO-curves were obtained near threshold to tones at levels of 35, 45 and 50 dB SPL. CF of the unit was 591 Hz and SR was 37 spikes/s. The left column represents the period histograms for the separate levels, 35, 45, 50 dB SPL from bottom to top. The middle column shows the IO-curves for these levels plotted in the same way as in Fig. 3B. Each IO-curve was derived from the responses to one level of the rate-level curve. Panels A–F and H use the same vertical scale. Obviously, the IO-curves provide considerably more information than the rate-level curve (G) in the corresponding range. The stars in panels D–F represent SR, and are in agreement with the instantaneous discharge rates for zero instantaneous sound pressure for each IO-curve. The IO-curves are replotted in one panel (H) using the same scale. The responses for 35, 45, and 50 dB overlie nicely and appear to represent the same IO relationship.

IO-curves overlap at relatively low stimulus levels (Fig. 6A). However, at higher stimulus levels IO-curves separate (Fig. 6B) and hysteresis is evident, almost certainly a consequence of the asymmetry of the period histograms along the temporal scale, which is usually attributed to refractory effects (Gray, 1967; Schroeder and Hall, 1974).

A comparison with traditional rate-level curves, an example of which is shown in Fig. 6C, indicates that IO-curves begin to diverge at levels well below average discharge rate saturation. This may be attributed to refractory behavior and/or to a change of the gain of the cochlear amplifier. It is of interest, however, that the gradual saturation of the average rate is not reflected in the shapes of static IO-curves which are expansive at all stimulus levels. Rather, saturation of the average discharge rate results in a scaling down of the instantaneous rate; in other words, the instantaneous rate in response to each instantaneous pressure is reduced when the stimulus level is increased. A reduction of the gain of the cochlear amplifier would result in a compression of the IO-curves in the horizontal direction. This appears to be the case at high levels (Fig. 6B and E).

To rule out the possibility that saturation in instantaneous-rate-vs-instantaneous-pressure curves might be obscured by the use of the linear abscissa, a subset of the data plotted in Fig. 6A and B was re-plotted on a logarithmic horizontal scale. For this purpose we could only use the data with instantaneous pressure greater than zero, since the logarithm of a negative value is not defined. This turns the horizontal scale in essence into a dB-scale and makes the curves directly comparable with average rate-level curves. These plots are shown in Fig. 6D and E where no evidence of response saturation was observed.

Data collected here were acquired in response to frequencies to which ANFs usually phase lock strongly. However, data were also collected for high CF ANFs in response to moderately low stimulus frequencies where phase-locking is observed but reduced in strength relative to responses to lower stimulus frequencies (Palmer and Russell, 1986; Joris et al., 1994). This is shown in Fig. 7 for an ANF with a CF of 17 kHz and a low SR (0.2 spikes/s). When stimulated with a 2 kHz tone-burst (i.e. in the tail of the ANF's tuning curve, and therefore, requiring high stimulus levels), IO-curves did not collapse onto the same trajectory. For the higher

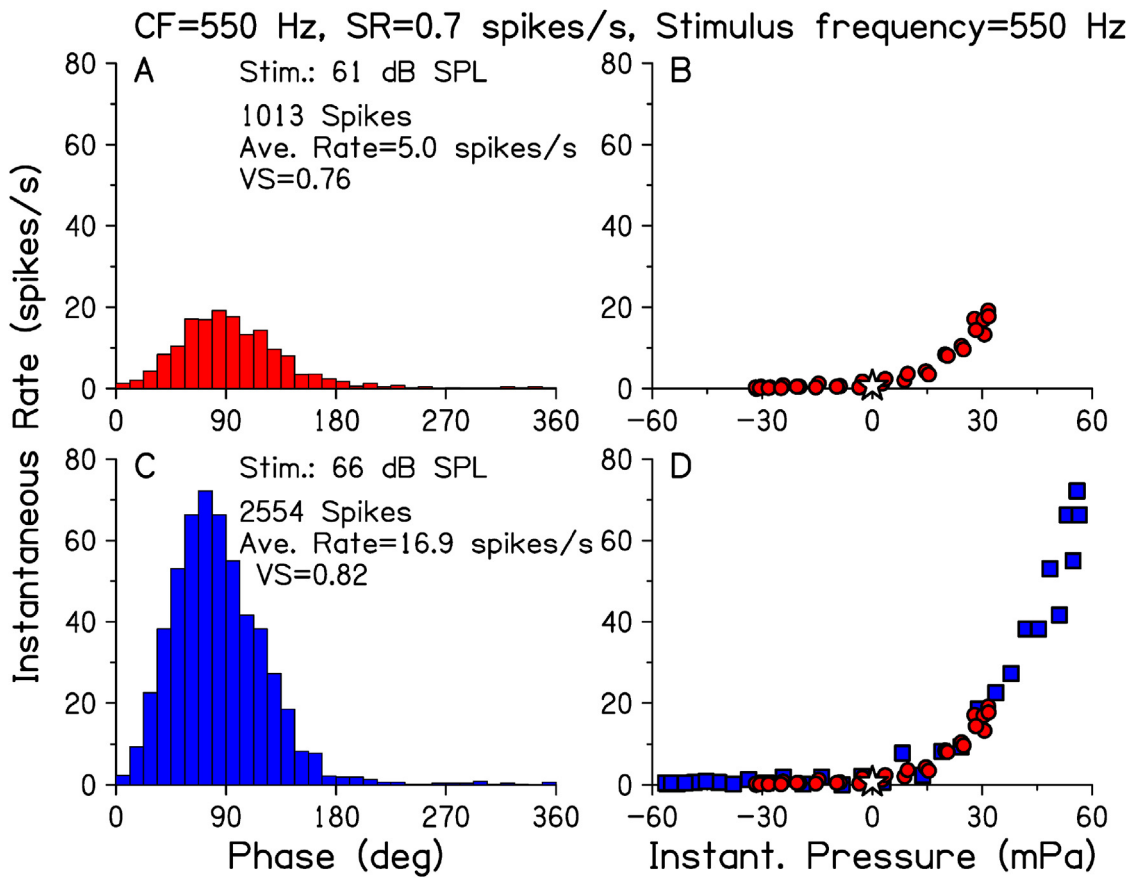

Fig. 5. Period histograms and IO-curves obtained near rate threshold are shown for a unit with a low SR of 0.7 spikes/s. The stimuli were tones at the CF (550 Hz) and at levels of 61 dB SPL (top row) and 66 dB SPL (bottom row). The average discharge rates were 5.0 and 16.9 spikes/s, respectively. Collecting data at lower levels that resulted only in modulation of the spontaneous discharge rate, would have required impractically long stimulation times. Period histograms are shown in the left column for 61 dB SPL (A) and for 66 dB SPL (C). B, D: IO-curves derived from the corresponding histograms. In D, the responses to both stimulus levels are shown; they overlap nicely, apparently representing the same IO-curve. The stars indicate SR. As in the case of the high SR unit shown in Fig. 4, SR agrees nicely with the instantaneous discharge rates for zero sound pressure of the individual IO-curves.

stimulus level, the IO-curve tilts upward compared to the IO curve derived from the lower level stimulus. Note that average driven rates for the two levels shown, 3.8 and 14.7 spikes/s, were far below rates required for saturation. In the case of saturation, the curve acquired at the higher stimulus level would have been scaled down as shown in Fig. 6B. The upward shift of the IO curve is in agreement with the increase of average discharge rate at higher frequencies as levels are raised.

4. Discussion

4.1. General

In this paper, we present a novel method designed to represent inner ear IO behavior in a static context by showing that data contained in single period histograms generated in response to low frequency, low level stimuli can be translated into IO curves that relate instantaneous stimulus pressure to instantaneous discharge rate. One key feature of this approach is that the forms of IO-curves representing different stimulus levels are similar at low levels and can be described by a single static IO-curve, i.e. the IO-relation is level- and time-invariant. The time-invariance of this system is reflected in the temporal-symmetry of period histograms. In addition, the SR (a static response) is in agreement with the instantaneous discharge rate in response to zero instantaneous input. The agreement between these measures supports the view that SR is the response to the null stimulus. It is also contrary to the view that a response to a tone is the sum of the spontaneous activity and the specific response to that tone (Sachs and Abbas, 1974; Sachs et al., 1989; Yates et al., 1990).

Limitations associated with the overall utility of the approach described here include the observation that IO-curves dissociate; i.e., break into multiple curve segments, when based on higher discharge rate responses and, therefore, high stimulus levels cannot be used to derive inner ear input-output properties using a single curve. Higher levels result in an IO-curve that is “scaled down” compared to IO-curves derived from lower level stimuli. An additional complication when dealing with higher discharge rates is IO-curve hysteresis, meaning that the output is dependent on the immediately preceding events and the relation between input and output is not time-invariant at higher levels of stimulation. The hysteresis observed in this study is well understood and is generally attributed to refractory effects. The “scaling down” phenomenon observed in IO-curves derived from high level stimuli is likely to have two causes. First, it may be caused by refractory effects, that is, the more often an ANF fires, a longer time is spent in a refractory state and the greater the chance of not responding to the stimulus. A second possible cause is the compressive nonlinear behavior of basilar membrane displacement (Rhode, 1978).

4.2. Responses at low and intermediate stimulus levels

Several efforts to model inner ear input-output relationships have been based on average discharge rate responses to relatively

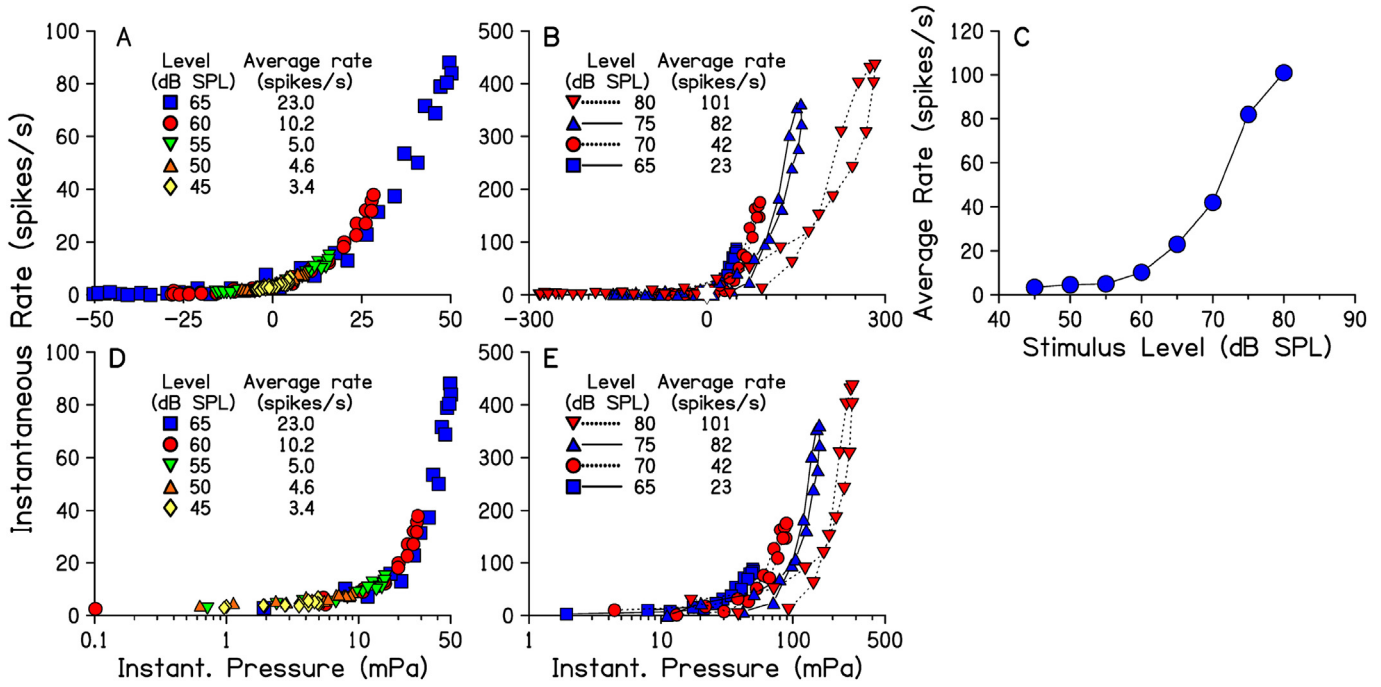

Fig. 6. Input-output curves for a large range of levels are shown. A–B: Instantaneous rates as a function of instantaneous sound pressure plotted on a linear scale are shown for lower level stimuli (45–65 dB SPL) in A and for 65–80 dB SPL in B. C: Average discharge rate as a function of sound pressure level is plotted for comparison. D–E: Instantaneous rates as a function of instantaneous sound pressure shown in panels A–B are replotted on a logarithmic scale. A, D: IO-curves constructed using lower level stimuli (45–65 dB SPL) show good overlap, regardless of the scale used. In contrast, IO-curves derived from higher level stimuli (B, E) do not overlap; this is likely a consequence of refractory effects. These curves do not show saturation in contrast to the rate-level curve (C). Using a logarithmic scale as shown in panel E does not introduce saturation of the instantaneous IO-curves. This ANF had a CF of approximately 500 Hz and a spontaneous rate of 3.2 spikes/s.

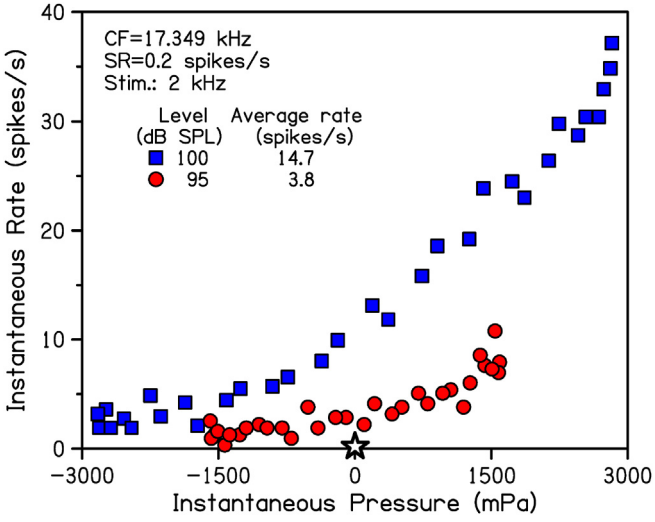

Fig. 7. Input-output curves derived from a high-CF ANF are shown in response to a relatively high frequency stimulus. This unit had a CF of 17.349 kHz and a spontaneous rate of 0.2 spikes/s. It was stimulated at 2.0 kHz in the tail of the tuning curve at 95 and 100 dB SPL. Note the difference between the IO-curves. The star represents the spontaneous rate.

long duration tonal stimulation (i.e., many cycles of a periodic signal) produced by varying stimulus levels throughout an ANF's dynamic range, and stimulus waveform properties have been completely and explicitly ignored. In such models, the stimulus driven rate is added to the spontaneous rate and Heil et al. (2011) have termed this type of model the rate-additivity model. Heil et al. (2011) also presented an alternative to this model in which amplitudes are used instead of rates, the amplitude-additivity model. The spontaneous rate is assumed to be caused by a resting stimulus with amplitude P_0 and the model responds to the sum of the amplitudes P_0 and the amplitude of the stimulus. Heil et al. (2011) do not make clear, however, whether they are using the instantaneous amplitude, the maximum amplitude or some fixed, averaged version of the amplitude (e.g. the effective pressure). Their comparison with the rate-additivity model suggests that they use a fixed amplitude. This assumption is strengthened by the maximum rates presented in their model results, which do not exceed those derived from the rate-additivity model. In contrast, maximum instantaneous rates can be much higher. On the other hand, their model has to accept negative values for the stimulus amplitude in order to explain spike rates lower than the spontaneous rate, which would be impossible in the case of the maximum amplitude or an averaged version of the amplitude. The method considered in the present report also uses average response values, although in this method, spike activity is considered within individual bins of the period histogram, each with a fixed temporal relation with respect to stimulus phase. Again, it is useful to note that the instantaneous rate represented in a given period histogram bin may be substantially higher than the overall average discharge rate produced in response to a long-duration tone. This is shown, for example, in Fig. 4 in which instantaneous rates as high as 120 spikes/s were recorded, whereas the overall average rate was just slightly higher than the SR, which was 37 spikes/s. This finding, also shown before by Johnson (1980), may have encoding relevance when considering rapidly changing acoustic conditions.

Rate-intensity curves have been studied in detail by Geisler (1990) and Müller et al. (1991) for ANFs exhibiting various SRs. Geisler (1990) explains the data of Geisler et al. (1985) by means of a two-stage model. The first stage is a static nonlinearity based on the measured intensity-voltage characteristic of inner hair cells. The second stage, representing action-potential generation, is

linear for high-SR ANFs, but a squaring function best described action potential generation for low- and medium-SR ANFs. Müller et al. (1991) also found that a square-law best describes the relation between mean discharge rate and effective sound pressure. For responses near threshold this would imply a linear relation between average discharge rate and stimulus intensity. From their data, they concluded that a simple square law is an accurate description of the underlying synaptic drive to all primary ANFs. For ANFs with very low spontaneous discharge rates, their data analyses led to the description of “negative spontaneous rate."

However, since a negative spontaneous rate cannot exist, its use is worrisome. Greenwood (1988) incorporated it into his model of responses to complex tones from Horst et al. (1986a, b). Yates et al. (1990) needed it also to model rate-level curves for low-SR ANFs. Even if one would imagine a negative spontaneous rate, this would be manifest in the shape of a period histogram. In order to overcome a negative spontaneous rate, a certain positive pressure would be required to elicit a response, i.e. a hard threshold is required. This should manifest itself in the form of center-clipping in the period histogram. For instantaneous IO-curves, that would mean that the output would be zero for negative and zero pressures and only start growing above zero for pressures above the threshold. Our data do not show such behavior nor have we found any indication in the literature of center-clipping in period histograms.

One goal of this investigation was to shed light on the response properties of ANFs with different SRs to tonal and complex stimuli near response threshold. In data from Horst et al. (1986b, 1990), instantaneous rates produced by small amplitude features of complex waveforms are commonly undervalued in low-SR ANFs. In agreement with this, the present data based on pure-tone stimuli show a stronger expansive behavior in low-SR ANFs near threshold than in medium-SR and high-SR ANFs. The term “expansive” as used here refers to an increasing IO-curve slope with increasing input. In Fig. 4, the slope increases with a factor of 2 for the instantaneous rate ranging from a spontaneous rate of 37 spikes/s to approximately 120 spikes/s, a roughly three-fold rate increment. While an increase in slope for this high-SRANF is evident, a much stronger increase in the slope of the curve representing a low-SR ANF is shown in Fig. 5; the slope increases by a factor of 18, ranging from the spontaneous rate, 0.7 spikes/s, to about 72 spikes/s. This was a general finding for low-SR ANFs.

4.3. General description of ANF IO-curves

While it is clear that IO curves representing low-SR ANFs grow expansively, even high-SR ANFs exhibit a degree of expansive behavior. For stimulus levels near synchronization thresholds, the increase in slope is small but clear. In addition, although higher levels of stimulation do not produce a single, static IO-curve, the curves do demonstrate clear expansive behavior. Thus, the idea of half wave rectification (Anderson, 1973; Sachs, 1984) is not supported by our data. In models of the auditory system, the relation between input and output has been described by a variety of relations; e.g., a power function (Meddis, 1986), an arctangent (Heinz et al., 2001) and an exponential function. The exponential relation was used, amongst others, by Siebert (1970), who based the formulation on Evans (1968) unpublished work, Colburn (1973), Littlefield (1973), Johnson (1974) and Goldstein and Srulovicz (1977). The present data provide actual experimental, quantitative evidence for the relevance of that assumption, as will be shown below.

Rate-level curves have been modeled such that the effective rate (average rate minus spontaneous rate) more or less mimics the magnitude of basilar membrane displacement (Geisler, 1990; Sachs et al., 1989; Yates et al., 1990). In these applications, SR is handled as a separate quantity that represents an intrinsic property of individual ANFs. The present approach offers a more parsimonious description of ANF responses, in that SR is viewed as an integral aspect of the IO-behavior of the IHC-ANF complex. The average rate is determined by spike activity of an ANF integrated over time. The asymmetry of the IO-curve around zero input causes an increase of average rate with increasing stimulus level. In this respect, our data give direct qualitative support for the IO-curve that Meddis (1986) used to model IHC membrane permeability. There exists, however, a difference in the actual shape of IO-curves proposed by Meddis and those described here. Meddis described a curve which is linear around zero input and compressive for intermediate and large inputs. Our data indicate that response growth is expansive in character throughout an ANF's dynamic range.

Because ANFs of different spontaneous rates (and hence, thresholds) innervate the same inner hair cell (Liberman, 1982; Wu et al., 2016), the search for the biological basis underlying functional differences has focused primarily on the IHC-afferent fiber synapse. Although different SR fibers vary morphologically (Liberman, 1980) and contact different regions of the IHC (Merchan-Perez and Liberman, 1996), presynaptic ribbons are highly variable in shape, size and associated number of synaptic vesicles (Liberman, 1980; Moser et al., 2006; Kantardzhieva et al., 2013). Interestingly, the size of presynaptic ribbon synapses relative to the size of associated glutamate receptor patches observed on the postsynaptic membrane are reciprocally related in the mouse (Liberman et al., 2011) but positively correlated in the gerbil (Zhang et al., 2018). Furthermore, the voltage-dependence and amplitude of presynaptic calcium influx in the active zone of the synapse are highly heterogeneous (Frank et al., 2009), as is the number of calcium channels (Wong et al., 2013). These findings offer compelling evidence in support of an argument that SR is determined by the molecular composition of each synapse, although other influences such as the effect of the lateral olivocochlear projection to afferent dendrites (Yin et al., 2014), cannot be ruled out.

To assess how the properties of synapses might shape the form of IO curves, consider an IO-curve exhibiting compression as shown in Fig. 8A in which a basic sigmoid curve passing through the origin is presented. This is modeled by means of a tangent hyperbolic. Such an IO-curve produces a symmetric output and little if any distortion for small inputs. If we consider a system that can only produce a positive response (e.g., an instantaneous discharge rate), this IO-curve would yield zero spontaneous rate and produce half-wave rectification. In Fig. 8B, the IO-curve is shifted both vertically (upwards) and horizontally (sideways). A curve like this is comparable to the profile of the ionic conductance of stereocilia as a function of ciliary displacement (Kros et al., 1995) except for the precise shape of the upper part of the curve. If we approximate the relation between stimulus waveform and stereociliary displacement as being linear (Khanna et al., 1991; Géléoc et al., 1979), the relation between stereociliary displacement and conductance as sigmoidal, and the relation between conductance and receptor potential as linear, which is most likely the case for small inputs (Zeddies and Siegel, 2004), the shape of the curve shown in Fig. 8B may be used as representative of the IO-relation between the instantaneous stimulus value and the receptor potential, as indicated in the left ordinate of the figure.

Furthermore, if we assume that every value of the receptor potential as presented in Fig. 8B induces a positive chance, however small, for the occurrence of a spike, we introduce the effective spike-generating potential by taking the lower horizontal asymptote of the receptor potential as the new reference. This results in a scale for the effective spike generating potential, as indicated along

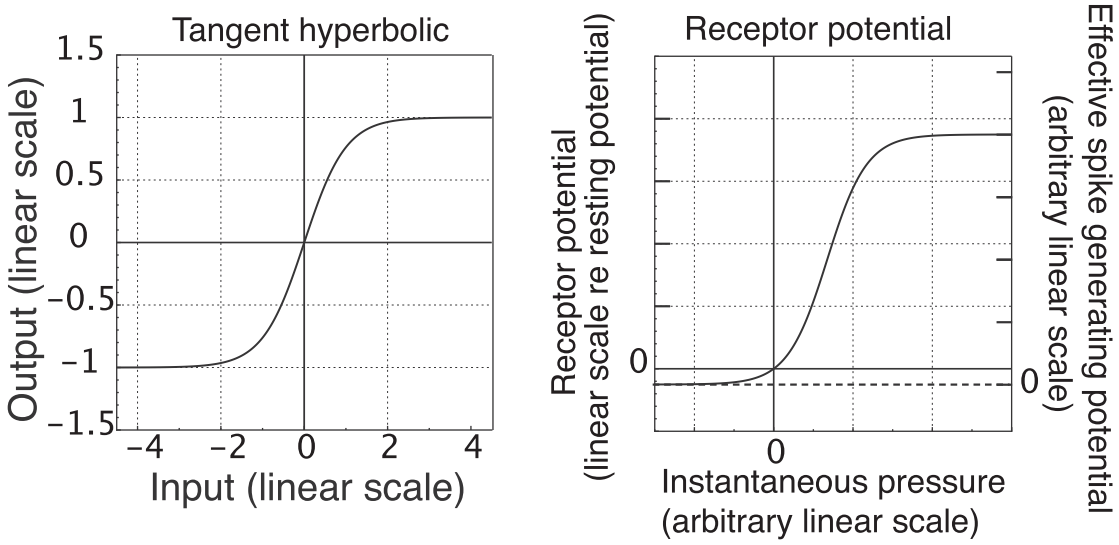

Fig. 8. Schematic illustrations of idealized input-output curves are shown. A: The curve represents a tangent hyperbolic. B: The curve represents the receptor potential of an inner hair cell as a function of instantaneous sound pressure, generated by shifting the tangent hyperbolic horizontally and upwards (left vertical scale). On the right vertical scale, the corresponding effective spike generating potential can be considered, with the lower asymptote of the receptor potential representing baseline.

the right ordinate of the figure. As a result, only positive spontaneous rates can occur (i.e., negative SRs are not defined), along with soft rectification. In this description, the spontaneous rate is not an isolated quality of the ANF but the response of the IHC-nerve-fiber complex to the null stimulus.

To describe the effective differences between high-, medium-, and low-SR fibers, we will consider two manipulations; first, shifting the IO curve shown in Fig. 8B in either the horizontal or vertical direction, and second, attenuating or multiplying in the horizontal or vertical direction. A shift of the IO-curve to the right (Horst et al., 1990) results in a decrease in SR. Although this provides an adequate description of certain qualitative aspects of single fiber responses, there are quantitative dilemmas with this interpretation. For intermediate inputs, a horizontal shift would result in a steeper curve when plotted on a logarithmic vertical scale. It would also produce steeper rate-level curves and there is no support for this in the literature. A downward shift in the vertical direction would also produce a decrease in SR, as well as negative instantaneous rates and some degree of rectification. Since negative discharge rates have no physical meaning, a downward shift cannot be defined from a biological perspective. Thus, neither a horizontal shift nor a vertical shift of the IO-curve provides a realistic description of the difference in behavior between high-SR and low-SR fibers.

A compression of the curve in the vertical direction would produce a smaller discharge rate for any input pressure (i.e., an attenuation of the output), while maintaining the basic shape of the curve. Varying the magnitude of compression would also create situations in which ANFs express different spontaneous rates (i.e. the response to the null stimulus), as is observed empirically. It also is consistent with the observation that for low- and medium-SR fibers, larger inputs are required to yield a given response. Consequently, it also adheres to the observation that progressively higher thresholds are required for medium- and low-SR fibers, respectively. Attenuation (i.e. a compression of the curve) in the horizontal direction would leave the average spontaneous rate unaltered but produce larger instantaneous rates; i.e., the slopes of IO curves would increase, producing differences in sensitivities, and consequently, thresholds of different ANFs.

In the following, we show that both effects (horizontal and vertical scaling) are represented in our data and can be characterized quantitatively. To that end, we examined the expansive character of IO-curves to determine whether this feature can be described by an exponential function. This was indeed the case as shown in Fig. 9 by re-plotting the data on a logarithmic vertical scale. Clearly, IO curves are linear, regardless of spontaneous rate. The data for the low-SR fiber shown here exhibit considerable spread as a consequence of the small number of spikes that were collected in the bins in the valleys of the period histograms, but

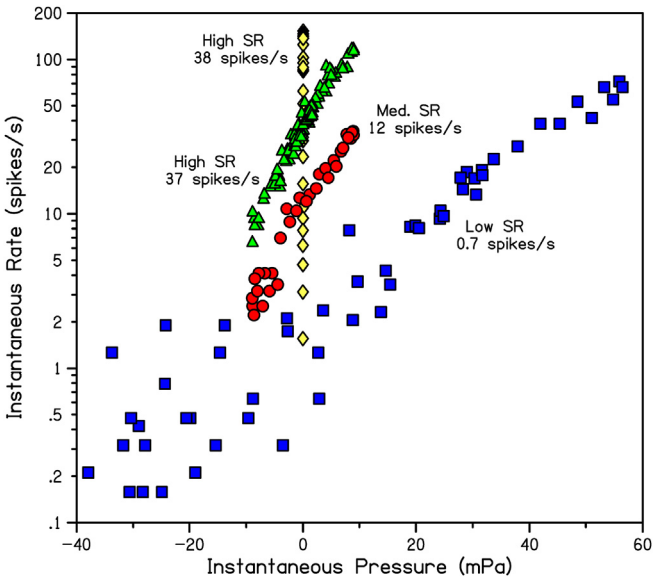

Fig. 9. The IO-curves shown in Fig. 3 (medium SR of 12 spikes/s), Fig. 4 (high SR of 37 spikes/s), and Fig. 5 (low SR of 0.7 spikes/s) are replotted using a logarithmic vertical scale. The linear relations shown suggest an exponential relation between the instantaneous pressure and the instantaneous discharge rate. This relation can be described by a slope α and the spontaneous rate R_{spont}. A higher spontaneous rate corresponds to an upward shift of the curve. Responses from another high-SR ANF (38 spikes/s) with a lower threshold are also shown. Note that the slope of the IO-curve for the ANF with the lower threshold is steeper than the slope of the IO-curve with the higher threshold.

they do cluster around a straight line.

This implies a parsimonious description of the data by the relation:

$$Inst.rate = R_{spont}e^{\alpha p} \quad (3)$$

or, taking the natural logarithm,

$$\log(Inst.rate) = \log(R_{spont}) + \alpha p \quad (4)$$

These calculations lead us to conclude that the thorough analysis of period histograms provides quantitative support for the exponential function described in modeling work. Relation (3) aptly describes responses of ANFs near threshold by means of only two parameters, R_{spont} and α. R_{spont} scales the instantaneous rate term, whereas α determines how the instantaneous rate varies with instantaneous sound pressure. Therefore, α is a measure of the sensitivity of the ANF and, as reasoned above, it should be expected that this sensitivity is related to the ANF's threshold. We assessed this by fitting straight lines to the data according to equation (4). This yielded estimates of the slope α. These values are plotted in Fig. 10 as a function of rate threshold for all the ANFs whose data were used in this investigation. These data encompass a large range of thresholds and the figure clearly shows how α decreases with increasing threshold, i.e. the smaller α is, the larger instantaneous pressures must be to evoke measurable responses.

Expressions (3) and (4) help us understand why low-SR ANFs exhibit a more expansive behavior than high-SR ANFs. These expressions imply that the response to the zero crossings of the stimulus yield an instantaneous rate equal to the spontaneous rate, as was shown in data presented here. Thus, we can divide a period histogram into an upper part with instantaneous rates above SR and a lower part with instantaneous rates below SR. The upper bound of the instantaneous rate is influenced by the refractory behavior of the ANF. In the simplified case of a period histogram exhibiting the shape of a half-wave rectified sinusoid, the instantaneous rate has a maximum value of π times the average rate (AR) (Horst et al., 1990). This means that the instantaneous rate in the upper part of the period histogram can vary between R_{spont} and πAR. In the case of ANFs with high SR, the instantaneous rate would vary between a minimum value of 18 spikes/s and a maximum value of about 650 spikes/s, a ratio of at most ~35. In the case of low-SR ANFs, the instantaneous would vary between less than 1 spike/s and also about 650 spikes/s, a ratio of more than 650. This means that low-SR ANFs have more than ten times the range available for variation of instantaneous rate than high-SR ANFs. As a consequence, low-SR fibers will use a considerably larger part of the IO-curve, thereby revealing a larger part of the exponential function. Consequently, among high-SR ANFs, the available range of the exponential IO-function is much smaller than among low-SR fibers, and, since reduction of a nonlinear function to a smaller interval renders it more linear, the input-output behavior of ANFs with high SR exhibit a more linear behavior than ANFs with low SR. This explains why low-SR ANFs are more expansive than high-SR fibers. Finally, although period histograms do not precisely exhibit the shape of half-wave rectified sinusoids, as confirmed in data presented here, that does not alter the basic reasoning advanced by our findings.

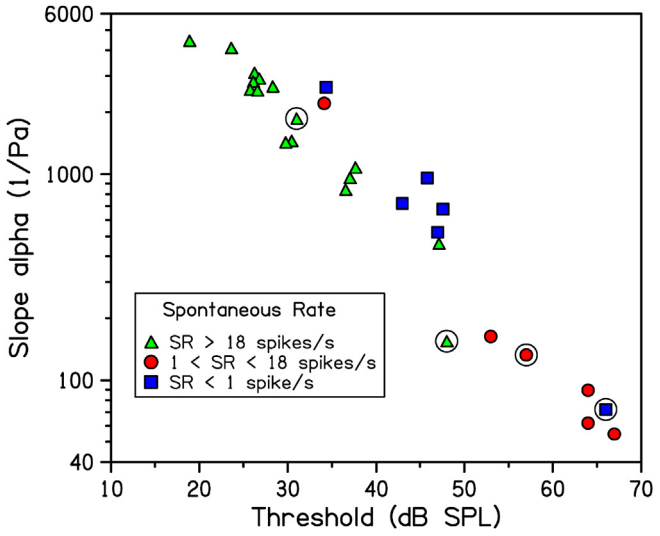

Fig. 10. The variable, alpha, is plotted as a function of the threshold for each ANF. Alpha is the slope of the IO-curve plotted on a logarithmic vertical scale. The encircled symbols represent the ANFs that produced the data for Fig. 9. Triangles represent low-SR ANFs (<1 spike/s), circles represent medium-SR ANFs (1 < SR < 18 spikes/s) and squares represent high-SR ANFs (>18 spikes/s).

4.4. Relation of ANF IO-curves with IHC data

According to relations (3) and (4), the ANF IO data can be described in a relatively simple way using only two parameters, R_{spont} and α and a relatively simple model, the sandwich model (e.g. Van Dijk et al., 1994), can explain this. The basic features of the model include a bandpass filter representing place-dependent mechanical filtering in combination with the gain caused by outer hair cell motility, a static nonlinearity representing transduction by stereocilia of inner hair cells, and a low-pass filter representing filtering in the basolateral membrane of inner hair cells. The static nonlinearity can be reasonably well-described by the Boltzmann function[2]:

$$y = \frac{y_{\max}}{1 + e^{-\alpha p + b}}$$

For small inputs, i.e. $\alpha p << b$, this can be approximated by the exponential relation:

$$y = y_{\max}e^{\alpha p - b}$$

or

$$y = ce^{\alpha p} \quad where \quad c = y_{\max}e^{-b}$$

This can explain the exponential nature of outputs in the lower part of the static nonlinearity. In this model, the expansive behavior of the data can be attributed to transduction in the apical part of the hair cell. For low-frequency stimuli, the non-sinusoidal shape of the response is not greatly altered by the low-pass filter properties of the basolateral membrane. Synaptic transmission can be described by a nonhomogeneous Poisson process (e.g. Siebert, 1970; Carney, 1993). This results in a fairly linear relation between the output of the low-pass filter and the period histogram. That means that the main influence of synaptic transmission on the shape of the period histogram is incorporated in the scalar c, i.e. is dependent only on gain. Differences in spontaneous rate are thus a consequence of differences in gain in different synapses. This brings us to the extension of the sandwich model presented in Fig. 11.

[2] The Boltzmann function and the tangent hyperbolic are closely related:

$$\frac{1}{1 + e^{-\alpha x + b}} = \{\tanh[(\alpha x - b)/2] + 1\}/2$$

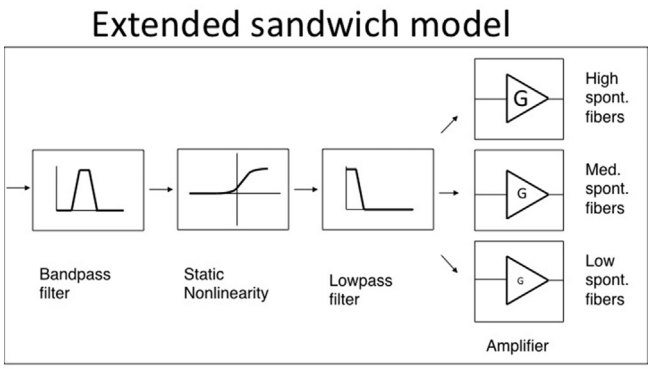

Fig. 11. The extended sandwich model consists of a bandpass filter representing mechanical filtering along the basilar membrane, a static nonlinearity representing transduction in the apical part of the inner hair cells, low-pass filtering in the basolateral membrane of the inner hair cells, and synapses with various gains producing ANFs with different spontaneous rates.

In earlier models, mechanoelectric transduction in the stereocilia was described by the Boltzmann function in accordance with the two-state gating spring model (Howard and Hudspeth, 1988). Meddis (2006) used a variation, the three-state gating spring model. Zhang et al. (2001) and Zilany and Bruce (2006) described the transduction by means of an input-output function that is expansive for negative input, compressive for positive input and linear around zero input. This is basically different from an exponential input-output function and from the Boltzmann function. In addition, an important subject of the various models is adaptation of the responses to stimuli of various levels (e.g. Zilany et al., 2009). It is unlikely that adaptation plays an important role in the responses presented here, as the average rates were either small, in the case of the low-SR fibers, or hardly different from spontaneous rates in the case of the high-SR fibers.

This sandwich model does not take into account the details of the several stages of transduction in the hair cell following mechano-electrical transduction. Such aspects have been modeled in more elaborate terms that take into account capacitance and conductance of the inner hair cell's membrane, voltage-gated potassium channels (Lopez-Poveda and Eustaquio-Martín, 2006; Zeddies and Siegel, 2004), voltage dependent calcium channels, and neurotransmitter management (e.g. Schroeder and Hall, 1974; Meddis, 1986; Carney, 1993). There is still uncertainty as to which extent these stages contribute to the nonlinearity of the relation between the input and output signal. Neubauer and Heil (2008), for example, show that for high frequency ANFs with low-SR the first-spike latency can be described by the third power of the stimulus pressure envelope. The attraction of their model is the relation between the third power and the conjunction of three independent sub-events leading to transmitter release. An important difference with the present study is that we did not consider the envelope of the stimulus and response but instead the fine structure. Also Neubauer and Heil (2008) assume that the envelope of the signal present in the hair cell before the low-pass filter is linearly related to the original stimulus, i.e. they ignore the influence of mechano-electrical transduction on the precise shape of the envelope. It is not clear how incorporation of mechano-electrical transduction would influence their model results. Nevertheless, it cannot be excluded from consideration that stages of transduction in the inner hair cell might add to the expansive relation between stimulus and ANF-response. Therefore, it would be useful in modeling studies of the IHCs to determine the input-output relations of each of the various stages.

5. Conclusions

(1) We have presented a relatively simple method to assess the static IO-relation that describes transduction from stimulus to spike generation on time scales shorter than the stimulus period.
(2) Spontaneous activity can be regarded as the response to the null-stimulus, i.e. it is equal to the instantaneous response caused by the zero crossings of a dynamic stimulus.
(3) On a linear scale, responses of low-SR ANFs show stronger expansive behavior than responses of high-SR ANFs.
(4) For all spontaneous rates, responses near threshold can be adequately described by an exponential relation.
(5) The exponential relation can at least partially be attributed to the lower part of the static nonlinearity associated with transduction in the apical part of the hair cells.
(6) Differences between fibers of different spontaneous rates can be modeled as decreasing gain for decreasing spontaneous rates of ANFs.

Acknowledgments

The interpretation of the single fiber data came about in the long run after many stimulating and insightful discussions. We like to thank in particular Steve Neely, Laurel Carney, Steven Colburn, Diek Duifhuis and Tobias Moser for their part in these discussions. We appreciate the thoughtful input from the reviewers. Software for analysis was programmed by Greg Suing and Tom Creutz.

This research did not receive any specific grant from funding agencies in the public, commercial, or not-for-profit sectors.

References

Anderson, D.J., 1973. Quantitative model for the effects of stimulus frequency upon synchronization of auditory nerve discharges. J. Acoust. Soc. Am. 54, 361–364.
Carney, L.H., 1993. A model for the responses of low-frequency auditory-nerve fibers in cat. J. Acoust. Soc. Am. 93, 401–417.
Colburn, H.S., 1973. Theory of binaural interaction based on auditory-nerve data. I. General strategy and preliminary results on interaural discrimination. J. Acoust. Soc. Am. 54, 1458–1470.
Dreyer, A., Delgutte, B., 2006. Phase locking of auditory-nerve fibers to the envelopes of high-frequency sounds: implications for sound localization. J. Neurophysiol. 96, 2327–2341.
Evans, J.E., 1968. Characterization of Synchronization to Low-frequency Tones by Fibers in the Cat's Auditory Nerve (unpublished).
Frank, T., Khimich, D., Neef, A., Moser, T., 2009. Mechanisms contributing to synaptic Ca2+ signals and their heterogeneity in hair cells. Proc. Natl. Acad. Sci. U.S.A. 106, 4483–4488.
Geisler, C.D., 1990. Evidence for expansive power functions in the generation of the discharges of 'low- and medium spontaneous' auditory-nerve fibers. Hear. Res. 44, 1–12.
Geisler, C.D., Deng, L., Greenberg, S.R., 1985. Thresholds for primary auditory fibers using statistically defined criteria. J. Acoust. Soc. Am. 77, 1102–1109.
Geisler, C.D., Silkes, S.M., 1991. Responses of "lower-spontaneous-rate" auditory-nerve fibers to speech syllables presented in noise. II: glottal-pulse periodicities. J. Acoust. Soc. Am. 90, 3140–3148.
Géléoc, G.S.G., Lennan, G.W.T., Richardson, G.P., Kros, C.J., 1979. A quantitative comparison of mechanoelectrical transduction in vestibular and auditory hair cells of neonatal mice. Proc. Roy. Soc. Lond. B 264, 611–621.
Goldstein, J.H., Srulovicz, P., 1977. Auditory-nerve spike intervals as an adequate basis for aural frequency measurement. In: Evans, E.F., Wilson, J.P. (Eds.), Psychophysics and Physiology of Hearing. Academic Press, London, pp. 337–346.
Gray, P.R., 1967. Conditional probability analyses of the spike activity of single neurons. Biophys. J. 7, 759–777.
Greenwood, D.D., 1988. Cochlear nonlinearity and gain control as determinants of the response of primary auditory neurons to harmonic complexes. Hear. Res. 32, 207–253.
Heil, P., Neubauer, H., Irvine, D.R.F., 2011. An improved model for the rate–level functions of auditory-nerve fibers. J. Neurosci. 31, 15424–15437.
Heinz, M.G., Colburn, H.S., Carney, L.H., 2001. Evaluating auditory performance limits: I. One-parameter discrimination using a computational model for the auditory nerve. Neural Comput. 13, 2273–2316.
Horst, J.W., Javel, E., Farley, G.R., 1986a. Effects of phase and amplitude spectrum in the nonlinear processing of complex stimuli in single fibers of the auditory nerve. In: Moore, Brian C.J., Patterson, Roy D. (Eds.), Auditory Frequency

Selectivity. Plenum Publishing Corporation, London, pp. 229–239.
Horst, J.W., Javel, E., Farley, G.R., 1986b. Coding of spectral fine structure in the auditory nerve. I. Fourier analysis of period and interspike interval histograms. J. Acoust. Soc. Am. 79, 398–416.
Horst, J.W., Javel, E., Farley, G.R., 1990. Coding of spectral fine structure in the auditory nerve. II: level-dependent nonlinear responses. J. Acoust. Soc. Am. 88, 2656–2681.
Howard, J., Hudspeth, A.J., 1988. Compliance of the hair bundle associated with gating of mechanoelectrical transduction channels in the bullfrog's saccular hair cell. Neuron 1, 189–199.
Johnson, D.H., 1974. The Response of Single Auditory-nerve Fibers in the Cat to Single Tones: Synchrony and Average Discharge Rate. Ph.D. thesis. Department of Electrical Engineering, Massachusetts Institute of Technology, Cambridge, Massachusetts.
Johnson, D.H., 1980. The relationship between spike rate and synchrony in responses of auditory-nerve fibers to single tones. J. Acoust. Soc. Am. 68, 1115–1122.
Joris, P.X., Smith, P.H., Yin, T.C.T., 1994. Enhancement of neural synchronization in the anteroventral cochlear nucleus. II. Responses in the tuning curve tail. J. Neurophysiol. 71, 1037–1051.
Kantardzhieva, A., Liberman, M.C., Sewell, W.F., 2013. Quantitative analysis of ribbons, vesicles, and cisterns at the cat inner hair cell synapse: correlations with spontaneous rat. J. Comp. Neurol. 521, 3260–3271.
Khanna, S.M., Ulfendahl, M., Flack, Å., 1991. Level dependence of cellular responses in the Guinea-pig cochlea. In: Duifhuis, H., Horst, J.W., van Dijk, P., van Netten, S.M. (Eds.), Biophysics of Hair Cell Sensory Systems. World Scientific, Singapore, pp. 266–271.
Kiang, N.Y.S., Watanabe, T., Thomas, E.C., Clark, L.F., 1965. Discharge Patterns of Single Fibers in the Cat's Auditory Nerve. MIT Research Monograph 35. MIT Press, Cambridge, MA.
Kros, C.J., Lennan, G.W.T., Richardson, G.P., 1995. Transducer currents and bundle movements in outer hair cells of neonatal mice. In: Flock, Å., Ottoson, D., Ulfendahl, M. (Eds.), Active Hearing. Elsevier, Oxford, pp. 113–125.
Liberman, M.C., 1978. Auditory-nerve response from cats raised in a low-noise chamber. J. Acoust. Soc. Am. 63, 442–455.
Liberman, M.C., 1980. Morphological differences among radial afferent fibers in the cat cochlea: an electron microscopic study of serial sections. Hear. Res. 3, 45–63.
Liberman, M.C., 1982. Single-neuron labeling in the cat auditory nerve. Science 216, 1239–1241.
Liberman, M.C., Dodds, L.W., Pierce, S., 1990. Afferent and efferent innervation of the cat cochlea: quantitative analysis with light and electron microscopy. J. Comp. Neurol. 301, 443–460.
Liberman, L.D., Wang, H., Liberman, M.C., 2011. Opposing gradients of ribbon size and AMPA receptor expression underlie sensitivity differences among cochlear-nerve/hair-cell synapses. J. Neurosci. 31, 801–808.
Littlefield, W.M., 1973. Investigation of the Linear Range of the Peripheral Auditory System (D.Sc. Thesis) St. Louis, MO. Xerox University Microfilms, Ann Arbor, MI.
Lopez-Poveda, E.A., Eustaquio-Martín, A., 2006. A biophysical model of the inner hair cell: the contribution of potassium currents to peripheral auditory compression. J. Assoc. Res. Otolaryngol 7, 218–235.
McGee, J.D., 1983. Phase-locking as a Frequency and Intensity Coding Mechanism in ANFs. M.Sc. thesis. Creighton University, Omaha, NE.
Merchan-Perez, A., Liberman, M.C., 1996. Ultrastructural differences among afferent synapses on cochlear hair cells: correlations with spontaneous discharge rate. J. Comp. Neurol. 371, 208–221.
Meddis, R., 1986. Simulation of mechanical to neural transduction in the auditory receptor. J. Acoust. Soc. Am. 79, 702–711.
Meddis, R., 2006. Auditory-nerve first-spike latency and auditory absolute threshold: a computer model. J. Acoust. Soc. Am. 119, 406–417.
Moser, T., Neef, A., Khimich, D., 2006. Mechanisms underlying the temporal precision of sound coding at the inner hair cell ribbon synapse. J. Physiol. 576, 55–62.
Müller, M., Robertson, M., Yates, G.K., 1991. Rate-versus-level functions of primary auditory nerve fibres: evidence for square law behaviour of all fibre categories in the Guinea pig. Hear. Res. 55, 50–56.
Neubauer, H., Heil, P., 2008. A physiological model for the stimulus dependence of first-spike latency of auditory-nerve fibers. Brain Res. 1220, 208–223.
Palmer, A.R., Russell, I.J., 1986. Phase-locking in the cochlear nerve of the Guinea pig and its relation to the receptor potential of inner hair-cells. Hear. Res. 24, 1–15.
Rhode, W.S., 1978. Some observations on cochlear mechanics. J. Acoust. Soc. Am. 64, 158–176.
Rose, J.E., Brugge, J.F., Anderson, D.J., Hind, J.E., 1967. Phase-locked response to low-frequency tones in single ANFs of the squirrel monkey. J. Neurophysiol. 30, 769–793.
Sachs, M.B., 1984. Neural coding of complex sounds: speech. Annu. Rev. Physiol. 46, 261–273.
Sachs, M.B., Abbas, P.J., 1974. Rate versus level functions for ANFs in cats: tone burst stimulation. J. Acoust. Soc. Am. 56, 1835–1847.
Sachs, M.B., Winslow, R.L., Sokolowski, B.H., 1989. A computational model for rate level functions from cat auditory-nerve fibers. Hear. Res. 41, 61–69.
Schroeder, M.R., Hall, J.L., 1974. Model for mechanical to neural transduction in the auditory receptor. J. Acoust. Soc. Am. 55, 1055–1060.
Siebert, W.M., 1970. Frequency discrimination in the auditory system: place or periodicity mechanisms. Proc. IEEE 58, 723–730.
Spoendlin, H., 1973. The innervation of the cochlea receptor. In: Moller, A.R. (Ed.), Mechanisms in Hearing. Academic Press, New York, pp. 185–229.
Temchin, A.N., Ruggero, M.A., 2010. Phase-locked responses to tones of chinchilla auditory nerve fibers: implications for apical cochlear mechanics. J. Assoc. Res. Otolaryngol 11, 297–318.
Van Dijk, P., Wit, H.P., Segenhout, J.M., Tubis, A., 1994. Wiener kernel analysis of inner ear function in the American bullfrog. J. Acoust. Soc. Am. 95, 904–919.
Winter, I.M., Robertson, D., Yates, G.K., 1990. Diversity of characteristic frequency rate-intensity functions in Guinea pig auditory nerve fibres. Hear. Res. 45, 191–202.
Wong, A.B., Jing, Z., Rutherford, M.A., Frank, T., Strenzke, N., Moser, T., 2013. Concurrent maturation of inner hair cell synaptic Ca2+ influx and auditory nerve spontaneous activity around hearing onset in mice. J. Neurosci. 33, 10661–10666.
Wu, J.S., Young, E.D., Glowatzki, E., 2016. Maturation of spontaneous firing properties after hearing onset in rat ANFs: spontaneous rates, refractoriness, and interfiber correlations. J. Neurosci. 36, 10584–10597.
Yates, G.K., Winter, I.M., Robertson, D., 1990. Basilar membrane nonlinearity and its influence on auditory nerve rate-intensity functions. Hear. Res. 50, 145–162.
Yin, Y., Liberman, L.D., Maison, S.F., Liberman, M.C., 2014. Olivocochlear innervation maintains the normal modiolar-pillar and habenular-cuticular gradients in cochlear synaptic morphology. J. Assoc. Res. Otolaryngol 15, 571–583.
Zeddies, D.G., Siegel, J.H., 2004. A biophysical model of an inner hair cell. J. Acoust. Soc. Am. 116, 426–441.
Zhang, L., Engler, S., Koepcke, L., Steenken, F., Köppl, C., 2018. Concurrent gradients of ribbon volume and AMPA-receptor patch volume in cochlear afferent synapses on gerbil inner hair cells. Hear. Res. 364, 81–89.
Zhang, X., Heinz, M.G., Bruce, I.C., Carney, L.H., 2001. A phenomenological model for the responses of auditory-nerve fibers. I. Nonlinear tuning with compression and suppression. J. Acoust. Soc. Am. 109, 648–670.
Zilany, M.S., Bruce, I.C., 2006. Modeling auditory-nerve responses for high sound pressure levels in the normal and impaired auditory periphery. J. Acoust. Soc. Am. 120, 1446–1466.
Zilany, M.S., Bruce, I.C., Nelson, P.C., Carney, L.H., 2009. A phenomenological model of the synapse between the inner hair cell and auditory nerve: long-term adaptation with power-law dynamics. J. Acoust. Soc. Am. 126, 2390–2412.